J. Mech. Phys. Solids 156 (2021) 104619

Contents lists available at ScienceDirect

Journal of the Mechanics and Physics of Solids

journal homepage: www.elsevier.com/locate/jmps

An analytical solution to the stress fields of kinked cracks

Zhuo-Er Liu [a,b], Yujie Wei [a,b,*]

[a] LNM, Institute of Mechanics, Chinese Academy of Sciences, Beijing 100190, China
[b] School of Engineering Sciences, University of Chinese Academy of Sciences, Beijing 100049, China

ARTICLE INFO

Keywords:
Kinked cracks
Stress fields
Stress intensity factors
Crack deflection
Fracture mechanics

ABSTRACT

Propagating cracks may deflect due to dynamic instability, running into pre-existing weak regions of heterogeneous media, or encountering variation in driving forces. The mechanical analysis of a kinked crack is of engineering significance for safety control and crack-network formation. Existing theories for kinked cracks relied on the perturbation method, as befit small kinks. The stress intensity factors (SIFs) are valid in the close proximity of the primary crack tip. As to the stress field of a kinked crack, it remains unsolved so far. In this work we develop an analytical solution to the stress fields of kinked cracks. By employing the conformal mapping and the Muskhelishvili approach, the close-form solution works for arbitrarily sized kinked cracks. The analytical theory is then validated using finite-element simulations. With this prior knowledge, we analyze the dependence of crack deflection on loading conditions, critical energy release rate, and the geometry of a kinked crack. We further demonstrate that such an analytical approach paves the way to obtain the solution of multiple-kinked cracks.

1. Introduction

When cracks propagate in non-uniform stress fields or in heterogeneous media with internal discontinuities, they may deflect and kink (Cotterell and Rice, 1980). This phenomenon has gained a lot of attention for their significance in engineering practices, from crack path control in safety design to crack-network formation in nonconventional energy harvesting. The latter is evidently seen in the course of rapid progress in hydraulic fracking to exploit natural gas encapsulated in shales full of pre-existing cracks, pores and weak zones. A well-developed crack network for high permeability of fluids is important for high yield. More broadly scenarios for crack propagation and deflection can be found in advanced materials with abundant interfaces. Fracture in anisotropic materials is another domain rich of kinked cracks (Azhdari and Nemat-Nasser, 1992; Zhu and Yang, 1999). Therefore, understanding their crack path in the presence of a variety of serving conditions becomes essential.

A successful theoretical analysis on crack path is contingent on faithful fracture criteria (Griffith, 1921; Irwin, 1957; Rice, 1968) and a well understanding about the interaction of a primary or kinked crack with pre-existing microcracks or weak region. Those disruptions may be ubiquitously seen in shale (Lee et al., 2015) and composite materials. The most broadly accepted criterion for crack path selection is based on the maximum energy release rate in the propagating direction (Hussain et al., 1973), which may be conveniently formulated once the SIFs are known. Therefore, finding a way to accurately evaluate SIFs has been a core subject in fracture mechanics, and has received enduring interest from researchers of solid mechanics (Williams, 1957; Cotterell and Rice, 1980; Hayashi and Nemat-Nasser, 1981; Gao and Rice, 1986; Hutchinson, 1990; Fett et al., 2004; Zhao and Guo, 2012; Zhang et al., 2014;

* Corresponding author.
E-mail address: yujie_wei@lnm.imech.ac.cn (Y. Wei).

https://doi.org/10.1016/j.jmps.2021.104619
Received 9 June 2021; Received in revised form 24 July 2021; Accepted 20 August 2021
Available online 24 August 2021

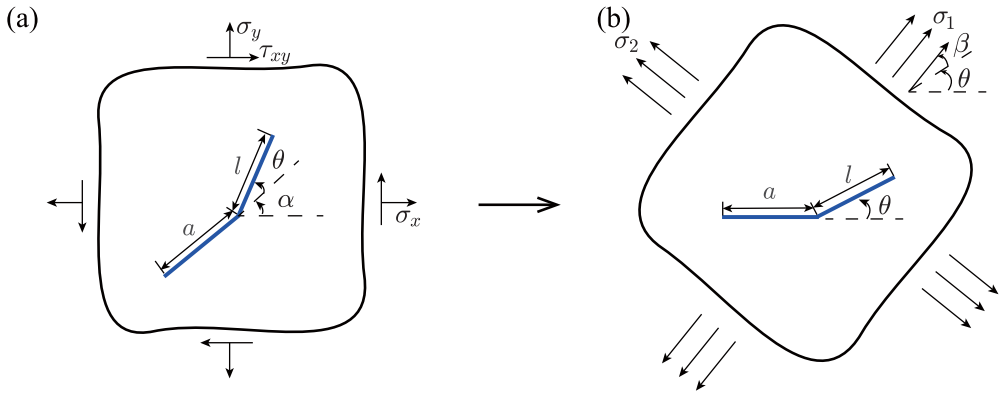

Fig. 1. A kinked crack and its transformation. (a) The crack with original part a forming an angle α with respect to x-axis, and the kinked part l characterized by angle θ. (b) We consider a configuration (after rotating clockwise the coordinate in (a) by angle α) so that the original part of the crack is horizontal. σ_1 and σ_2 are the principal stresses and β is the angle between σ_1 and the kinked part.

Salvadori and Fantoni, 2016; Yu et al., 2018; Leblond et al., 2019; Quaranta et al., 2019).

Based on the maximum strain energy release rate criteria, He and Hutchinson (1989) solved the fracture problem of crack deflection in two dissimilar isotropic materials. Hutchinson and Suo (1992) developed a comprehensive theory about crack propagation in layered materials. Very recently, Zeng and Wei (2017) gave the analytical formulae of crack deflection encountering heterogeneous interfaces in brittle media. It is fair to say that the field has gained quite profound knowledge, from both theories and experimental investigations, to understand the first deflection for an initially straight crack.

The extension of a kinked crack, a crack composed of two segments with the second part being misaligned with the first one, renders more challenges. In what follows we may refer to as a double-kinked crack. The crack tip SIFs may be inexorably modified by the presence of the second segment and consequentially the strain energy release rate along an arbitrary direction may subject to change. Earlier work dates back to Nuismer (1975), who gave the SIFs at the tip of an infinitesimal kinked crack. Lo (1978) gave an integral equation by regarding a crack as continuous distribution of dislocations to solve the SIFs at crack tips. Cotterell and Rice (1980) gave the SIFs of a slightly curved or kinked crack by using perturbation method based on Muskhelishvili approach (Muskhelishvili, 1953). He et al. (1991) gave an expression of SIFs at the tip of a finite kinked crack by considering the influence of T-stress. It is noted that these researches on the finite kinked cracks are aimed at short kinks (Li et al., 2018). People have to resort to numerical method to investigate more general case of finite kinks by utilizing the rapid development of computational power and numerical techniques. For instance, Rybicki and Kanninen (1977) developed a numerical way to calculate SIFs and energy release rate called virtual crack closure technique (VCCT) to understand the deflection of finite kinked cracks. Moes et al. (1999) developed extended finite element method (XFEM) to deal with the deflection of a kinked crack in materials with interior interfaces. Wei et al. (2009) used a dynamic FEM to simulate the three-dimensional crack propagation across a twist-misoriented grain boundary and investigated how crack-deflection may enhance fracture toughness of literally brittle materials. Numerical methods are also adopted to examine the hydraulic fracture (Zhang et al., 2007; Weng et al., 2011; Lecampion and Desroches, 2015; Zou et al., 2016) where kinked cracks may deflect in the influence of pre-existing cracks, bedding plane, geo-stresses, frictional effect and liquid-solid interaction (Zhang and Jeffrey, 2006; Bunger and Detournay, 2008; Chuprakov et al., 2014; Detournay, 2016; Zeng and Wei, 2016) and so on. Regardless the progress of mechancial analysis on kinked cracks, stress fields of a kinked crack remain unsolved so far.

In this paper, we seek to establish a theoretical framework to calculate the stress fields and SIFs of a kinked crack with arbitrary size. The work is organized as follows. We state the boundary-value problem (BVP) in Section 2, and adopt conformal mapping in order to obtain the corresponding complex analytical functions for the given BVP. In Section 3, the stress fields and SIFs are deduced from the complex analytical functions. Our method is verified with FE simulations and is compared with the existing theory by He et al. (1991). In Section 4, we apply the theory to analyze crack deflection of a double-kinked crack in brittle isotropic media. The mathematical approach is generalized to cracks of multiple kinks, as discussed in Section 5.

2. Complex analytical functions of a kinked crack

In contrast to the analysis by Zeng and Wei (2017) where a straight crack running into a weak region in brittle media was considered, here we focus on the stress fields and crack-tip SIFs of an arbitrarily sized kinked crack, and examine its deflection. As seen in Fig. 1a, the kinked crack has two arbitrary segments and the SIFs of the second segment is of our interest. In case of need, one may certainly be able to solve the SIFs of the free end of the other segment after proper coordinate transformation. The shape of a kinked crack is characterized by the length of the original crack a, the kinked part l and kink angle θ. Fig. 1b shows the crack after rotating clockwise the coordinate in Fig. 1a by an angle α.

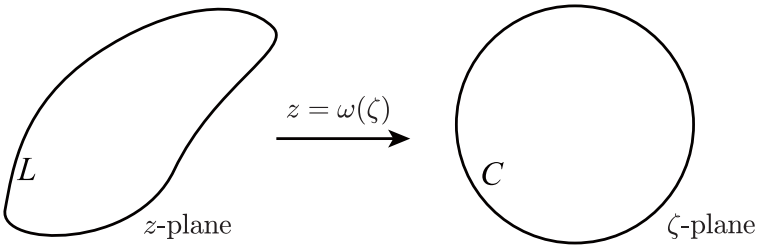

Fig. 2. A conformal mapping in the complex plane. The open region of the original boundary L in z-plane is mapping into the open region of the unit circle C in ζ-plane.

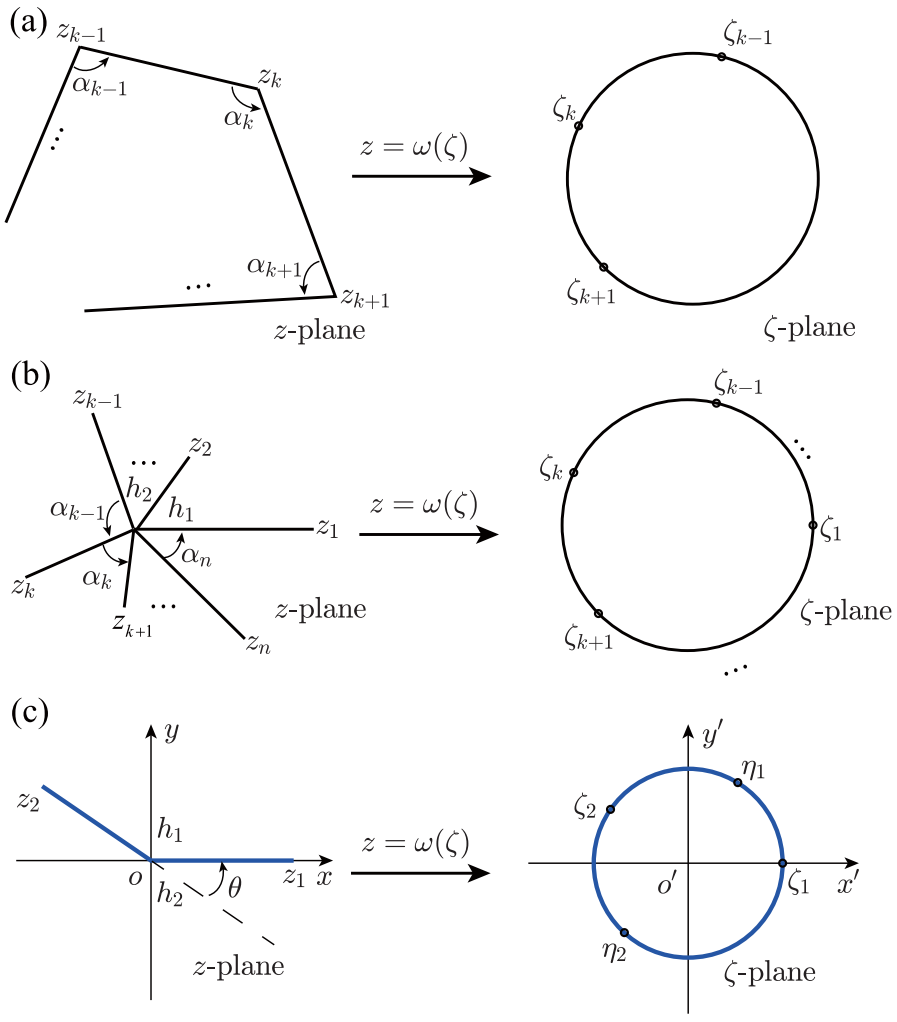

Fig. 3. Schwartz-Christoffel Integral conformal mapping between z-plane and ζ-plane. (a) A polygonal to unit circle mapping: The periphery of the polygon is projected to that of a circle, and points ζ_k on the unit circle correspond to vertices z_k of the polygon. The bounded and open regions of the circle correspond to those of the polygon, respectively. (b) Mapping a star-shaped region into a unit circle. The points ζ_k correspond to the free ends z_k. (c) Mapping a kinked crack into a unit circle. The two ends z_1 and z_2 of the crack and two joining points h_1 and h_2 are mapped to points ζ_1, ζ_2, η_1 and η_2, in turn, on the unit circle.

2.1. Conformal mapping

For the fracture problem shown in Fig. 1b, we assume the validity of linear elastic analysis. Following Muskhelishvili (1953), the stress fields for linear elastic plane problem can be described by two complex analytical functions $\varphi(z)$ and $\psi(z)$, which are connected

with planar stresses σ_x, σ_y and τ_{xy} as

$$\sigma_x + \sigma_y = 4\mathrm{Re}[\varphi'(z)] = 2[\varphi'(z) + \overline{\varphi'(z)}], \tag{1a}$$

$$\sigma_y - \sigma_x + 2i\tau_{xy} = 2[\bar{z}\varphi''(z) + \psi'(z)], \tag{1b}$$

where $\overline{(\cdot)}$ is the conjugate of $(\cdot)$, and $(\cdot)'$ and $(\cdot)''$ represent the first and the second derivative of $(\cdot)$ with respect to z, respectively and $z = x + iy$. For a general boundary L shown in Fig. 2, the boundary condition is given as

$$\varphi(z) + z\overline{\varphi^{prime}(z)} + \overline{\psi(z)} = i\left(F_x + iF_y\right) = f(s), \tag{2}$$

where $f(s)$ characterizes the stress on the boundary surface. However, due to the complexity of possible boundary conditions, conformal mapping is usually employed to elegantly simplify such problems. As shown in Fig. 2, we seek a transformation in the manner of $z = \omega(\zeta)$, where z is a point in z-plane and ζ is its counterpart in ζ-plane. To fully utilize the characteristics of complex functions, the boundary L in z-plane is usually mapped into a unit circle C in ζ-plane. After employing the conformal mapping $z = \omega(\zeta)$, the stress fields of a plane problem can now be written as

$$\sigma_\rho + \sigma_\theta = 2\left[\frac{\varphi'(\zeta)}{\omega'(\zeta)} + \overline{\frac{\varphi'(\zeta)}{\omega'(\zeta)}}\right], \tag{3a}$$

$$\sigma_\theta - \sigma_\rho + 2i\tau_{\rho\theta} = \frac{2\zeta^2}{\rho^2\overline{\omega'(\zeta)}}\left[\overline{\omega(\zeta)}\left(\frac{\varphi'(\zeta)}{\omega'(\zeta)}\right)' + \omega'(\zeta)\frac{\psi'(\zeta)}{\omega'(\zeta)}\right], \tag{3b}$$

where $\zeta = \rho e^{i\theta}$ is the variable in ζ-plane and $\varphi(\zeta)$ and $\psi(\zeta)$ are the corresponding complex analytical functions, and σ_ρ, σ_θ, and $\tau_{\rho\theta}$ are the radial stress, hoop stress and shear stress in the polar coordinate in ζ-plane. The BVP in ζ-plane is in the form of

$$\varphi(\xi) + \frac{\omega(\xi)}{\overline{\omega'(\xi)}}\overline{\varphi'(\xi)} + \overline{\psi(\xi)} = f(\xi). \tag{4a}$$

Its integral form is given as

$$\int_C \frac{\varphi(\xi)}{\xi - \zeta}\mathrm{d}\xi + \int_C \frac{\omega(\xi)}{\overline{\omega'(\xi)}}\frac{\overline{\varphi'(\xi)}}{\xi - \zeta}\mathrm{d}\xi + \int_C \frac{\overline{\psi(\xi)}}{\xi - \zeta}\mathrm{d}\xi = \int_C \frac{f(\xi)}{\xi - \zeta}\mathrm{d}\xi, \tag{4b}$$

where ξ is any point on the unit circle C. Therefore, finding an appropriate conformal mapping is of great significance in solving the BVP.

Here we adopt the Schwartz-Christoffel Integral to map the open region of a polygon into that of a unit circle (as shown in Fig. 3a) (Driscoll and Trefethen, 2002). The mapping is written in the form of

$$\omega(\zeta) = K_1\int\left[\prod_{k=1}^{n}\frac{(\zeta - \zeta_k)^{\frac{\alpha_k}{\pi}-1}}{\zeta^2}\right]\mathrm{d}\zeta + K_2, \tag{5a}$$

where ζ_k are associated with the connecting points (z_k in z-plane) and K_1, K_2 are two complex constants. There is a special case for Schwartz-Christoffel Integral, which maps a star-shaped domain to the open part of a unit circle (as shown in Fig. 3b) (Driscoll and Trefethen, 2002).

$$\omega(\zeta) = \frac{R}{\zeta}\prod_{k=1}^{n}(\zeta - \eta_k)^{\frac{\alpha_k}{\pi}}, \tag{5b}$$

where η_k in ζ-plane is the mapping of the centered point h_k of the k-th line, whose other end z_k is mapped to ζ_k in ζ-plane, and R is a complex parameter depending on η_k and ζ_k. For the kinked crack problem shown in Fig. 3c, there are four key points defining the two segments of the kinked crack in z-plane: the two free ends of the segments at $z_1 = l$ and $z_2 = ae^{i(\pi-\theta)}$ and the rest two joining ends at $h_1 = h_2 = 0$. The corresponding counterparts of these four points in ζ-plane are $\zeta_1 = e^{i\psi_1}$ and $\zeta_2 = e^{i\psi_2}$ for z_1 and z_2, respectively; and $\eta_1 = e^{i\varphi_1}$ and $\eta_2 = e^{i\varphi_2}$ for h_1 and h_2, in turn.

Back to Eq. (5a), we have $n = 4$. The corresponding angles of the points z_1, z_2, h_1 and h_2 in z-plane are $\alpha_1 = \alpha_2 = 2\pi$, $\alpha_3 = \pi - \theta$, and $\alpha_4 = \pi + \theta$, and their ζ-plane counterpoints are ζ_1, ζ_2, $\zeta_3 = \eta_1$, $\zeta_4 = \eta_2$, respectively. Eq. (5a) is therefore written as

$$\omega(\zeta) = K_1\int\left[\left(\frac{\zeta - \eta_1}{\zeta - \eta_2}\right)^{-\frac{\theta}{\pi}}\frac{(\zeta - \zeta_1)(\zeta - \zeta_2)}{\zeta^2}\right]\mathrm{d}\zeta + K_2. \tag{6a}$$

For the same token, we have $n = 2$ in Eq. (5b), $\alpha_1 = \pi - \theta$ and $\alpha_2 = \pi + \theta$. It can be reformulated as

$$\omega(\zeta) = \frac{R}{\zeta}(\zeta-\eta_1)^{\frac{\pi-\theta}{\pi}}(\zeta-\eta_2)^{\frac{\pi+\theta}{\pi}}. \tag{6b}$$

When mapping to the same circle in ζ-plane, the uniqueness of the mapping requires Eq. (6a) and (b) identical. Comparing the derivatives of Eq. (6a) and (b) with respect to ζ, we obtain

$$\frac{K_1}{R}(\zeta-\zeta_1)(\zeta-\zeta_2) = \zeta^2 + \frac{\theta}{\pi}(\eta_2-\eta_1)\zeta - \eta_1\eta_2. \tag{7}$$

Given the above equation holds for any ζ, we have $K_1 = R$,

$$\zeta_1 + \zeta_2 = \frac{\theta}{\pi}(\eta_1-\eta_2), \tag{8a}$$

and

$$\zeta_1\zeta_2 = -\eta_1\eta_2. \tag{8b}$$

Let $R = |R|e^{i\phi}$, $\zeta_j - \eta_k = r_{jk}e^{i\phi_{jk}}$. Substituting points ζ_1 and ζ_2 into Eq. (6b), we have

$$\omega(\zeta_1) = \frac{|R|e^{i\phi}}{e^{i\psi_1}}\left(r_{11}e^{i\phi_{11}}\right)^{\frac{\pi-\theta}{\pi}}\left(r_{12}e^{i\phi_{12}}\right)^{\frac{\pi+\theta}{\pi}} = l, \tag{9a}$$

and

$$\omega(\zeta_2) = \frac{|R|e^{i\phi}}{e^{i\psi_2}}\left(r_{21}e^{i\phi_{21}}\right)^{\frac{\pi-\theta}{\pi}}\left(r_{22}e^{i\phi_{22}}\right)^{\frac{\pi+\theta}{\pi}} = ae^{i(\pi-\theta)}, \tag{9b}$$

respectively. By comparing the modules of these two equations, we yield

$$\left(\frac{r_{11}}{r_{21}}\right)^{\frac{\pi-\theta}{\pi}}\left(\frac{r_{12}}{r_{22}}\right)^{\frac{\pi+\theta}{\pi}} = \frac{l}{a}. \tag{10}$$

Now we have four parameters and three independent equations. We can fix one parameter, then the other three can be fully determined. It is convenient to set $\zeta_1 = 1$ ($\psi_1 = 0$ as the starting point in ζ-plane). Physically, we only need to discuss φ_1 and φ_2 in the range of $\varphi_1 \in [0,\pi]$ and $\varphi_2 \in [\pi, 2\pi]$. With Eq. (8a) and (b), we obtain the following two equations

$$\frac{\theta}{\pi}(\sin\varphi_2 - \sin\varphi_1) = \sin(\varphi_1+\varphi_2), \tag{11a}$$

and

$$\frac{\theta}{\pi}(\cos\varphi_1 - \cos\varphi_2) = 1 - \cos(\varphi_1+\varphi_2). \tag{11b}$$

Eq. (10) can be rewritten as

$$\left(\frac{1-\cos\varphi_1}{1-\cos(\psi_2-\varphi_1)}\right)^{\frac{\pi-\theta}{2\pi}}\left(\frac{1-\cos\varphi_2}{1-\cos(\psi_2-\varphi_2)}\right)^{\frac{\pi+\theta}{2\pi}} = \frac{l}{a}. \tag{11c}$$

The four parameters ψ_1, ψ_2, φ_1 and φ_2 are then fully determined by solving Eq. (11). By substituting these parameters into Eq. (9), we have

$$|R| = \frac{l}{2(1-\cos\varphi_1)^{\frac{\pi-\theta}{2\pi}}(1-\cos\varphi_2)^{\frac{\pi+\theta}{2\pi}}} = \frac{a}{2[1-\cos(\psi_2-\varphi_1)]^{\frac{\pi-\theta}{2\pi}}[1-\cos(\psi_2-\varphi_2)]^{\frac{\pi+\theta}{2\pi}}}, \tag{12a}$$

and

$$\phi = \frac{\pi-\theta}{\pi}\arctan\frac{\sin\varphi_1}{1-\cos\varphi_1} + \frac{\pi+\theta}{\pi}\arctan\frac{\sin\varphi_2}{1-\cos\varphi_2}. \tag{12b}$$

Here we consider three special cases of a kinked crack.

(1) When $l/a = 0$, Eq. (11) can be readily solved, from which we have $\eta_1 = \eta_2 = 1$ and $\zeta_2 = -1$. Hence $\varphi_1 = 0$, $\varphi_2 = 2\pi$ and $\psi_2 = \pi$. Substituting the second term of the right-hand side of Eq. (12) into (6b), we obtain the mapping function as

$$\omega(\zeta) = \frac{ae^{-i\theta}}{4}\left(\zeta + \frac{1}{\zeta} - 2\right). \tag{13a}$$

(2) For $l/a = 1$, we solve Eq. (11) and obtain $\eta_1 = e^{i\arccos\frac{\theta}{\pi}}$, $\eta_2 = e^{i\left(\arccos\frac{\theta}{\pi}+\pi\right)}$ and $\zeta_2 = e^{2i\arccos\frac{\theta}{\pi}}$, from which we have $\varphi_1 = \arccos\frac{\theta}{\pi}$, $\varphi_2 = \arccos\frac{\theta}{\pi}+\pi$ and $\psi_2 = 2\arccos\frac{\theta}{\pi}$. Again, with known R, substituting Eq. (12) into (6b), we obtain the mapping function as

$$\omega(\zeta) = \frac{\pi a e^{i\left(\frac{\pi-\theta}{\pi}\arctan\sqrt{\frac{\pi+\theta}{\pi-\theta}}-\frac{\pi+\theta}{\pi}\arctan\sqrt{\frac{\pi-\theta}{\pi+\theta}}\right)}}{2(\pi-\theta)^{\frac{\pi-\theta}{2\pi}}(\pi+\theta)^{\frac{\pi+\theta}{2\pi}}\zeta}\left(\zeta - e^{i\arccos\frac{\theta}{\pi}}\right)^{\frac{\pi-\theta}{\pi}}\left(\zeta - e^{i\left(\arccos\frac{\theta}{\pi}+\pi\right)}\right)^{\frac{\pi+\theta}{\pi}}. \tag{13b}$$

(3) If $l/a \to \infty$, it is straightforward to find $\eta_1 = \eta_2 = \zeta_2 = -1$ by solving Eq. (11), and we have $\varphi_1 = \varphi_2 = \psi_2 = \pi$. Therefore,

$$\omega(\zeta) = \frac{l}{4}\left(\zeta + \frac{1}{\zeta} + 2\right). \tag{13c}$$

The conformal mapping enables us to seek the solution of the BVP beyond a unit circle other than in the region outside of a kinked crack.

2.2. Solutions for complex analytical functions

For a linear elastic plane problem, because of the single value of displacement, the complex analytical functions are given as (Muskhelishvili, 1953)

$$\varphi(\zeta) = -\frac{F_x + iF_y}{2\pi(1+\kappa)}\ln\omega(\zeta) + \Gamma_1\omega(\zeta) + \varphi_0(\zeta), \tag{14a}$$

$$\psi(\zeta) = \frac{\kappa\left(F_x - iF_y\right)}{2\pi(1+\kappa)}\ln\omega(\zeta) + \Gamma_2\omega(\zeta) + \psi_0(\zeta), \tag{14b}$$

where F_x and F_y are the forces acting on the crack surfaces, $\Gamma_1 = \frac{1}{4}(\sigma_1+\sigma_2)$ and $\Gamma_2 = -\frac{1}{2}(\sigma_1-\sigma_2)e^{-2i\beta}$ are the stresses at infinity. σ_1 and σ_2 are the principal stresses and β is the angle between σ_1 and the real axis. κ is a material constant related to the Poisson's ratio ν, $\kappa = 3-4\nu$ for plane strain deformation and $\kappa = \frac{3-\nu}{1+\nu}$ for plane stress. $\varphi_0(\zeta)$ and $\psi_0(\zeta)$ are the holomorphic functions outside of the unit circle. If the crack surfaces are free, $F_x = F_y = 0$. Substituting Eq. (14) into (4a) and note that $\varphi_0(\zeta)$, $\psi_0(\zeta)$ and $f_0(\zeta)$ also satisfy the boundary condition given in Eq. (4a), we have

$$f_0(\xi) = -\Gamma_1\omega(\xi) - \overline{\Gamma_1}\omega(\xi) - \overline{\Gamma_2\omega(\xi)}. \tag{15}$$

From the boundary condition given in Eq. (4b) we have

$$\varphi_0(\zeta) - \frac{1}{2\pi i}\int_C \frac{\omega(\xi)}{\overline{\omega'(\xi)}}\frac{\overline{\varphi_0'(\xi)}}{\xi-\zeta}d\xi = -\frac{1}{2\pi i}\int_C \frac{f_0(\xi)}{\xi-\zeta}d\xi. \tag{16}$$

By substituting Eqs. (6b) and (15) into (16) and employing the Cauchy Integral Formula, we get the solution of $\varphi_0(\zeta)$ as

$$\varphi_0(\zeta) = -\frac{1}{\zeta}\left(R\Gamma_1 + R\overline{\Gamma_1} + \overline{R\Gamma_2}\right). \tag{17}$$

And by substituting Eqs. (17) into (14a), we obtain one of the two complex analytical functions, $\varphi(\zeta)$, which is in the form of

$$\varphi(\zeta) = \frac{\Gamma_1 R}{\zeta}(\zeta-\eta_1)^{\frac{\pi-\theta}{\pi}}(\zeta-\eta_2)^{\frac{\pi+\theta}{\pi}} + \varphi_0(\zeta). \tag{18}$$

Then we consider the other complex potential function $\psi(\zeta)$ using the same method. By using the conjugate of the boundary condition Eq. (4a) we can obtain

$$\overline{\varphi(\xi)} + \frac{\overline{\omega(\xi)}}{\omega'(\xi)}\varphi'(\xi) + \psi(\xi) = \overline{f(\xi)}. \tag{19a}$$

Its integral form is given as

$$\int_C \frac{\overline{\varphi(\xi)}}{\xi-\zeta}d\xi + \int_C \frac{\overline{\omega(\xi)}}{\omega'(\xi)}\frac{\varphi'(\xi)}{\xi-\zeta}d\xi + \int_C \frac{\psi(\xi)}{\xi-\zeta}d\xi = \int_C \frac{\overline{f(\xi)}}{\xi-\zeta}d\xi, \tag{19b}$$

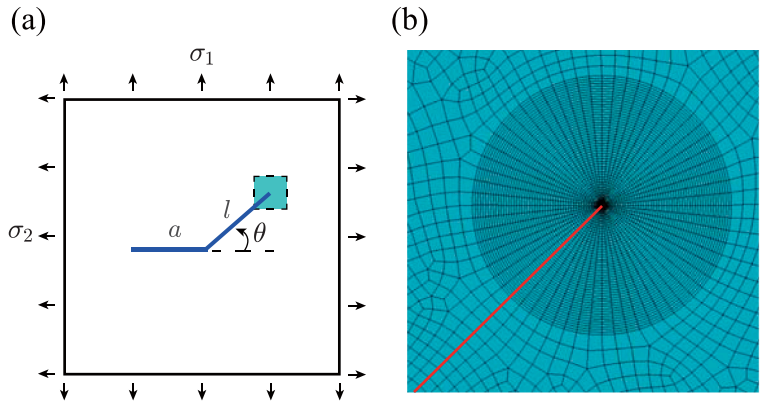

Fig. 4. The finite-element model for validation. (a) Boundary condition of a kinked crack. (b) Close-up view to show mesh near the crack tip (the red line is the crack surface).

The holomorphic term $\psi_0(\zeta)$ is determined by

$$\psi_0(\zeta) = -\frac{1}{2\pi i}\int_C \frac{\overline{f_0(\xi)}}{\xi-\zeta}\mathrm{d}\xi + \frac{1}{2\pi i}\int_C \overline{\frac{\omega(\xi)}{\omega'(\xi)}}\frac{\varphi_0'(\xi)}{\xi-\zeta}\mathrm{d}\xi. \tag{20}$$

By substituting Eqs. (6b) and (15) into (20) and employing the Cauchy Integral Formula, we get the solution of $\psi_0(\zeta)$ as

$$\psi_0(\zeta) = -\frac{1}{\zeta}\left(\overline{R\Gamma_1} + \overline{R}\Gamma_1 + R\Gamma_2\right) + \frac{R\Gamma_1 + R\overline{\Gamma_1} + \overline{R\Gamma_2}}{-\zeta + \frac{\zeta^2(\pi-\theta)}{\pi(\zeta-\eta_1)} + \frac{\zeta^2(\pi+\theta)}{\pi(\zeta-\eta_2)}}. \tag{21}$$

And by substituting Eq. (21) into (14b), we obtain the other complex analytical function $\psi(\zeta)$, which is in the form of

$$\psi(\zeta) = \frac{\Gamma_2 R}{\zeta}(\zeta-\eta_1)^{\frac{\pi-\theta}{\pi}}(\zeta-\eta_2)^{\frac{\pi+\theta}{\pi}} + \psi_0(\zeta). \tag{22}$$

We will show next that the stress fields and SIFs can be readily obtained with known $\varphi(\zeta)$ and $\psi(\zeta)$.

3. Stress fields at the tip of kinked cracks

With the two complex analytical functions $\varphi(\zeta)$ and $\psi(\zeta)$ given in Eqs. (18) and (22), respectively, we now proceed to derive the stress fields and SIFs of the kink tip in this section. The theoretical results will be validated using finite-element simulations.

3.1. Stress fields from complex analytical functions

Following Eq. (1), it is convenient to calculate the stress field around the tip of a kinked crack. For each point z in the z-plane, we can obtain the corresponding point ζ in ζ-plane from $z = \omega(\zeta)$. Let $\widetilde{\varphi}(z)$ and $\widetilde{\psi}(z)$ denote the complex analytical functions in z-plane, $\widetilde{\varphi}(z) = \widetilde{\varphi}[\omega(\zeta)] = \varphi(\zeta)$ and $\widetilde{\psi}(z) = \widetilde{\psi}[\omega(\zeta)] = \psi(\zeta)$. By using the rule of compound functions, we have $\widetilde{\varphi}'(z) = \frac{\varphi'(\zeta)}{\omega'(\zeta)}$, $\widetilde{\psi}'(z) = \frac{\psi'(\zeta)}{\omega'(\zeta)}$ and $\widetilde{\varphi}''(z) = \frac{\varphi''(\zeta)\omega'(\zeta) - \omega''(\zeta)\varphi'(\zeta)}{[\omega'(\zeta)]^3}$. Eq. (1) may be rewritten as

$$\sigma_x + \sigma_y = 4\mathrm{Re}\left[\frac{\varphi'(\zeta)}{\omega'(\zeta)}\right] = 2\left[\frac{\varphi'(\zeta)}{\omega'(\zeta)} + \overline{\frac{\varphi'(\zeta)}{\omega'(\zeta)}}\right], \tag{23a}$$

$$\sigma_y - \sigma_x + 2i\tau_{xy} = 2\left[\overline{\omega(\zeta)}\frac{\varphi''(\zeta)\omega'(\zeta) - \omega''(\zeta)\varphi'(\zeta)}{[\omega'(\zeta)]^3} + \frac{\psi'(\zeta)}{\omega'(\zeta)}\right]. \tag{23b}$$

The stress components at point $z = \omega(\zeta)$ are then given as

$$\sigma_x = \mathrm{Re}\left[\frac{\varphi'(\zeta)}{\omega'(\zeta)} + \overline{\frac{\varphi'(\zeta)}{\omega'(\zeta)}} - \overline{\omega(\zeta)}\frac{\varphi''(\zeta)\omega'(\zeta) - \omega''(\zeta)\varphi'(\zeta)}{[\omega'(\zeta)]^3} - \frac{\psi'(\zeta)}{\omega'(\zeta)}\right], \tag{24a}$$

$$\sigma_y = \mathrm{Re}\left[\frac{\varphi'(\zeta)}{\omega'(\zeta)} + \overline{\frac{\varphi'(\zeta)}{\omega'(\zeta)}} + \overline{\omega(\zeta)}\frac{\varphi''(\zeta)\omega'(\zeta) - \omega''(\zeta)\varphi'(\zeta)}{[\omega'(\zeta)]^3} + \frac{\psi'(\zeta)}{\omega'(\zeta)}\right], \tag{24b}$$

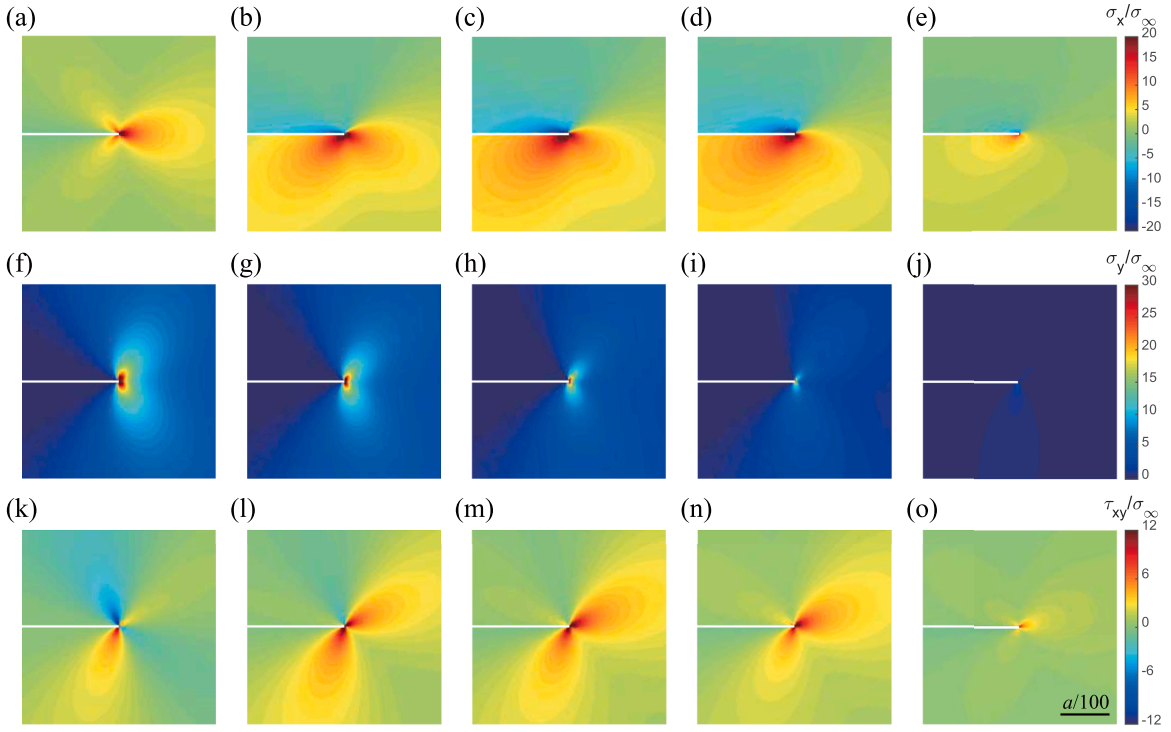

Fig. 5. Normalized stress components to show stress concentration around the tip of a kinked crack ($l = a$). The sample is subject to uniaxial stress (see Fig. 4a, here the white line is the crack surface). For each row, we show one stress component of samples with different kink angle $\theta = 0$, $\pi/6$, $\pi/4$, $\pi/3$ and $\pi/2$, in turn. (a)-(e) σ_x/σ_∞, (f)-(j) σ_y/σ_∞, and (k)-(o) τ_{xy}/σ_∞.

$$\tau_{xy} = \mathrm{Im}\left[\overline{\omega(\zeta)}\frac{\varphi''(\zeta)\omega'(\zeta) - \omega''(\zeta)\varphi'(\zeta)}{[\omega'(\zeta)]^3} + \frac{\psi'(\zeta)}{\omega'(\zeta)}\right], \tag{24c}$$

where $\omega(\zeta)$, $\varphi(\zeta)$ and $\psi(\zeta)$ are known from Eqs. (6b), (18) and (22), in turn.

By using Eq. (24) we can obtain the stress components of each point on z-plane. Here we take a special case for instance where a kinked crack is subject to uniaxial stress and its kinked part is of the same length to the original crack. The corresponding $\omega(\zeta)$ is given in Eq. (13b). The theoretical results are validated by using finite-element calculations. The applied boundary conditions (either uniaxial or biaxial) of the model are shown in Fig. 4a. We focus on the stress fields and the SIFs of the double-kinked crack tip, with close-up view to show the mech in Fig. 4b. We first consider the sample in Fig. 4a is subject to uniaxial stress, with $\sigma_1 = \sigma_\infty$ and $\sigma_2 = 0$. The normalized stress fields of different θ near the crack tip are shown in Fig. 5. For better view, we rotate the image counter-clockwisely by θ. Fig. 5a to e show σ_x/σ_∞ for $\theta = 0$, $\pi/6$, $\pi/4$, $\pi/3$ and $\pi/2$ in turn. The corresponding stress components of σ_y/σ_∞ and τ_{xy}/σ_∞, are shown in the second and the third row, respectively. When $\theta = 0$, the stress fields near the crack tip are the same as those of a straight crack.

3.2. SIFs of a kinked crack

The SIFs of a kinked crack can be readily determined from its stress fields. By substituting Eq. (14) into (3), we have

$$\sigma_\theta + i\tau_{\rho\theta} = \left[\frac{\Gamma_1\omega'(\zeta) + \varphi_0'(\zeta)}{\omega'(\zeta)} + \frac{\overline{\Gamma_1\omega'(\zeta) + \varphi_0'(\zeta)}}{\overline{\omega'(\zeta)}}\right] + \frac{\zeta^2}{\rho^2\overline{\omega'(\zeta)}}\left[\overline{\omega(\zeta)}\left(\Gamma_1 + \frac{\varphi_0'(\zeta)}{\omega'(\zeta)}\right)' + \Gamma_2\omega'(\zeta) + \psi_0'\right] \tag{25}$$

Employing the definition of SIFs, and substituting Eq. (20) into (25), we obtain the following expression for K_I and K_II in terms of ζ

$$\begin{aligned} K_\mathrm{I} + iK_\mathrm{II} = {} & \lim_{\zeta\to\zeta_1}\sqrt{2\pi[\omega(\zeta) - \omega(\zeta_1)]}(\sigma_\theta + i\tau_{\rho\theta}) = \lim_{\zeta\to\zeta_1}\sqrt{2\pi[\omega(\zeta) - \omega(\zeta_1)]} \\ & \left\{\left[\frac{\Gamma_1\omega'(\zeta) + \varphi'(\zeta)}{\omega'(\zeta)} + \frac{\overline{\Gamma_1\omega'(\zeta) + \varphi'(\zeta)}}{\overline{\omega'(\zeta)}}\right.\right. \\ & \left.\left. + \lim_{\zeta\to\zeta_1}\frac{\zeta^2}{\rho^2\overline{\omega'(\zeta)}}\left[\overline{\omega(\zeta)}\left(\frac{\varphi'(\zeta)}{\omega'(\zeta)}\right)' + \Gamma_2\omega'(\zeta) - \frac{1}{2\pi i}\left(\int_C\frac{\overline{f_0(\xi)}}{\xi - \zeta}\mathrm{d}\xi\right)' - \frac{1}{2\pi i}\left(\int_C\frac{\overline{\omega(\xi)}}{\omega'(\xi)}\frac{\varphi_0'(\xi)}{\xi - \zeta}\mathrm{d}\xi\right)'\right]\right]\right\} \end{aligned} . \tag{26}$$

Here we follow the tradition way to define K_{I} and K_{II} in terms of crack-tip stress fields and assume the validity of $1/\sqrt{r}$ singularity. Bear in mind we have

$$\lim_{\zeta\to\zeta_1}\frac{\sqrt{\omega(\zeta)-\omega(\zeta_1)}}{\omega'(\zeta)}=\lim_{\zeta\to\zeta_1}\frac{\sqrt{\frac{1}{2}\omega''(\zeta_1)(\zeta-\zeta_1)^2}}{\omega''(\zeta_1)(\zeta-\zeta_1)}=\frac{1}{\sqrt{2\omega''(\zeta_1)}} \tag{27a}$$

and

$$\lim_{\zeta\to\zeta_1}\frac{\sqrt{\omega(\zeta)-\omega(\zeta_1)}}{\overline{\omega'(\zeta)}}=\lim_{\zeta\to\zeta_1}\frac{\sqrt{\frac{1}{2}\omega''(\zeta_1)(\zeta-\zeta_1)^2}}{\overline{\omega''(\zeta_1)(\zeta-\zeta_1)}}=\frac{1}{\sqrt{2\overline{\omega''(\zeta_1)}}}. \tag{27b}$$

Substituting Eqs. (6b), (15), (17) and (27) into (26) and denoting $K=K_{\mathrm{I}}-iK_{\mathrm{II}}$ yields

$$K=\overline{K_{\mathrm{I}}+iK_{\mathrm{II}}}=2\sqrt{\pi}\,\frac{\varphi_0'(1)}{\sqrt{\omega''(1)}}=\frac{2\sqrt{\pi}\left(R\Gamma_1+R\overline{\Gamma_1}+\overline{R\Gamma_2}\right)}{\sqrt{R(1-\eta_1)^{\frac{\pi-\theta}{\pi}}(1-\eta_2)^{\frac{\pi+\theta}{\pi}}\left[2-\frac{2(\pi-\theta)}{\pi(1-\eta_1)}-\frac{2(\pi+\theta)}{\pi(1-\eta_2)}-\frac{\theta(\pi-\theta)}{\pi^2(1-\eta_1)^2}+\frac{2(\pi-\theta)(\pi+\theta)}{\pi^2(1-\eta_1)(1-\eta_2)}+\frac{\theta(\pi+\theta)}{\pi^2(1-\eta_2)^2}\right]}}. \tag{28}$$

In particular, its explicit expression can be given for three special cases.

(1) When $l/a=0$, we have

$$\begin{aligned}K&=\sqrt{\frac{\pi a}{2}}\left(\Gamma_1e^{-i\frac{\theta}{2}}+\overline{\Gamma_1}e^{-i\frac{\theta}{2}}+\overline{\Gamma_2}e^{i\frac{\theta}{2}}\right)\\&=\frac{1}{2}\sqrt{\frac{\pi a}{2}}\left[(\sigma_1+\sigma_2)\cos\frac{\theta}{2}-(\sigma_1-\sigma_2)\cos\left(\frac{\theta}{2}+2\beta\right)\right]-i\frac{1}{2}\sqrt{\frac{\pi a}{2}}\left[(\sigma_1+\sigma_2)\sin\frac{\theta}{2}+(\sigma_1-\sigma_2)\sin\left(\frac{\theta}{2}+2\beta\right)\right].\end{aligned} \tag{29a}$$

(2) When $l/a=1$, we have

$$K=\sqrt{\pi a}\left[(\Gamma_1+\overline{\Gamma_1})\frac{\pi e^{i\left(\frac{\pi-\theta}{\pi}\arctan\sqrt{\frac{\pi+\theta}{\pi-\theta}}-\frac{\pi+\theta}{\pi}\arctan\sqrt{\frac{\pi-\theta}{\pi+\theta}}\right)}}{(\pi-\theta)^{\frac{\pi-\theta}{2\pi}}(\pi+\theta)^{\frac{\pi+\theta}{2\pi}}}+\overline{\Gamma_2}\frac{\pi e^{i\left(\frac{\pi+\theta}{\pi}\arctan\sqrt{\frac{\pi-\theta}{\pi+\theta}}-\frac{\pi-\theta}{\pi}\arctan\sqrt{\frac{\pi+\theta}{\pi-\theta}}\right)}}{(\pi-\theta)^{\frac{\pi-\theta}{2\pi}}(\pi+\theta)^{\frac{\pi+\theta}{2\pi}}}\right]. \tag{29b}$$

(3) When $l/a\to\infty$, we have

$$K=\sqrt{\frac{\pi l}{2}}(\Gamma_1+\overline{\Gamma_1}+\overline{\Gamma_2})=\frac{1}{2}\sqrt{\frac{\pi l}{2}}[(\sigma_1+\sigma_2)-(\sigma_1-\sigma_2)\cos2\beta-i(\sigma_1-\sigma_2)\sin2\beta]. \tag{29c}$$

If one is only concerned with the SIFs of a kinked crack, we may obtain it without the necessity of deriving $\psi(\zeta)$. We illustrate in Appendix a convenient way on how to obtain the same expression for SIFs without knowing $\psi(\zeta)$.

3.3. Finite-element verification

As we briefly mentioned in the introduction, Nuismer (1975) gave the SIFs at the tip of an infinitesimal kinked crack. The work by Cotterell and Rice (1980) extended the analysis of SIFs for slightly curved or kinked crack, which was perturbation method based. Their formulae may only work for a small kinked part. By combining the T stress in the Williams (1957) with the results from Cotterell and Rice (1980), He et al. (1991) obtained the SIFs in the form of

$$K_{\mathrm{I}}=\int_0^l\sigma_\theta\sqrt{\frac{2}{\pi(l-r)}}dr=\frac{1}{2}\cos\frac{\theta}{2}(1+\cos\theta)k_{\mathrm{I}}-\frac{3}{2}\cos\frac{\theta}{2}\sin\theta k_{\mathrm{II}}+T\sqrt{\frac{8l}{\pi}}\sin^2\theta, \tag{30a}$$

$$K_{\mathrm{II}}=\int_0^l\tau_{\rho\theta}\sqrt{\frac{2}{\pi(l-r)}}dr=\frac{1}{2}\cos\frac{\theta}{2}\sin\theta k_{\mathrm{I}}+\frac{1}{2}\cos\frac{\theta}{2}(3\cos\theta-1)k_{\mathrm{II}}-T\sqrt{\frac{8l}{\pi}}\sin\theta\cos\theta. \tag{30b}$$

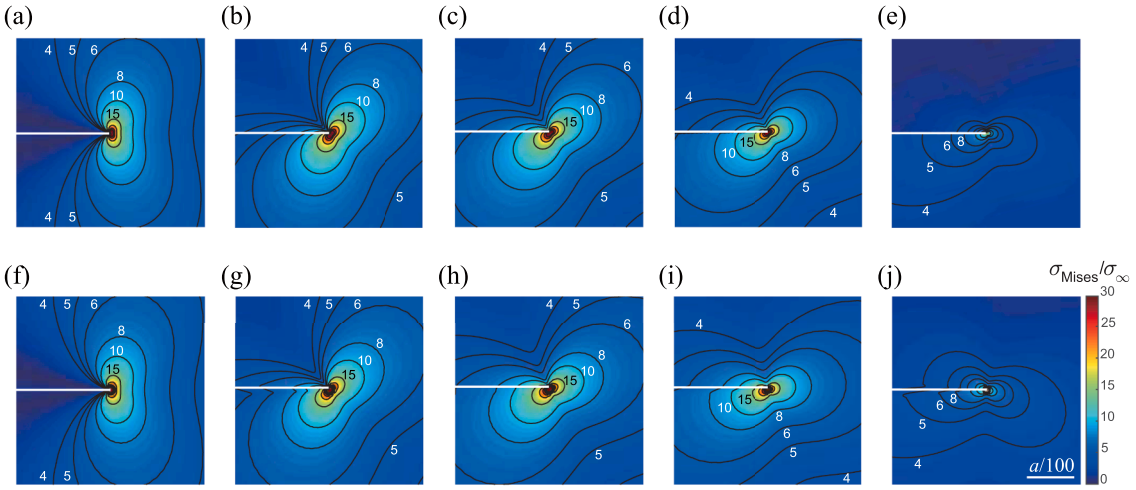

Fig. 6. A comparison of crack-tip stresses between theoretical solutions and FE simulations. Here we show the normalized Mises stress contours at the tip of a kinked crack. The geometries and boundary conditions are the same as those used in Fig. 5 (the white line represents the crack). In each row, we show $\sigma_{\text{Mises}}/\sigma_\infty$ of samples with different kink angle $\theta = 0, \pi/6, \pi/4, \pi/3$ and $\pi/2$, in turn. (a)-(e) Analytical solution given by Eq. (24); (f)-(j) the FE results.

Given the perturbation method may incur limitations of K_{I} and K_{II} for l, we examine the applicability of the theories by Cotterell and Rice (1980) and He et al. (1991) to double-kinked cracks of arbitrary size. Again, we adopt the FE model shown in Fig. 4, with $\sigma_1 = \sigma_\infty$ and $\sigma_2 = 0$ for uniaxial loading. We consider a sufficiently large sample by setting both sides of the sample to be $20a$. Two parts of the kinked crack is of the same length, i.e., $l/a = 1$. Stress singularity at the crack tip is captured by using collapsed elements with duplicate nodes in the shape of sweeping quadrilateral, as demonstrated in Fig. 4b. The crack-tip von Mises stress from our analytical solution for samples with $\theta = 0, \pi/6, \pi/4, \pi/3$ and $\pi/2$ are shown, in turn, from Fig. 6a to e. Those counterparts from FE simulations are shown in Fig. 6f to j. The solution given by Eq. (24) agrees well with the results from FE simulations.

For cracks subject to stresses shown in Fig. 4a, we have $\beta = \pi/2 - \theta$. Using Eq. (28) we can get the SIFs of a kinked crack of an arbitrary size. We show in Fig. 7 the SIFs as a function of l/a when the kinked crack is subject to uniaxial stress ($\sigma_2 = 0$). Here K_{I} and K_{II} as a function of l/a are shown in Fig. 7a and b, respectively. For biaxial stress status, ($\sigma_2 = 0.5\sigma_1$), we have K_{I} and K_{II} shown in Fig. 7c and d, respectively. It is seen that for different θ, our theoretical predictions are in line with FE results.

For particular geometries, we may obtain the explicit expression of both $\varphi(\zeta)$ and $\psi(\zeta)$. Subsequently, the SIFs may be in explicit form of θ, l and a. We demonstrate in this part by considering several l/a when the double-kinked crack in Fig. 4a is subject to uniaxial loading $\sigma_1 = \sigma$ and $\sigma_2 = 0$.

(1) When $l/a = 0$, we have

$$K_{\text{I}} - iK_{\text{II}} = \frac{1}{2}\sigma\sqrt{\frac{\pi a}{2}}\left(e^{-i\frac{\theta}{2}} + e^{-i\frac{3\theta}{2}}\right) = \sigma\sqrt{\frac{\pi a}{2}}\left[\frac{1}{2}\left(\cos\frac{\theta}{2} + \cos\frac{3\theta}{2}\right) - i\frac{1}{2}\left(\sin\frac{\theta}{2} + \sin\frac{3\theta}{2}\right)\right]. \tag{31a}$$

The variations of both K_{I} and K_{II} as a function of θ are shown Fig. 8a. While Eqn. (28) capture the trends of K_{I} and K_{II} as θ varies, the formula given by He et al. (1991) capture the FE results better. If we consider a case $l/a = 0.2$, both Eqn. (28) in this study and Eqn. (30) by He et al. (1991) capture the FE results well, as demonstrated in Fig. 8b.

(1) When $l/a = 1$, we have

$$K_{\text{I}} - iK_{\text{II}} = \sigma\sqrt{\pi a}\left[\frac{\pi e^{i\left(\frac{\pi-\theta}{\pi}\arctan\sqrt{\frac{\pi+\theta}{\pi-\theta}} - \frac{\pi+\theta}{\pi}\arctan\sqrt{\frac{\pi-\theta}{\pi+\theta}}\right)}}{2(\pi-\theta)^{\frac{\pi-\theta}{2\pi}}(\pi+\theta)^{\frac{\pi+\theta}{2\pi}}} + \frac{\pi e^{i\left(\frac{\pi+\theta}{\pi}\arctan\sqrt{\frac{\pi-\theta}{\pi+\theta}} - \frac{\pi-\theta}{\pi}\arctan\sqrt{\frac{\pi+\theta}{\pi-\theta}} - 2\theta\right)}}{2(\pi-\theta)^{\frac{\pi-\theta}{2\pi}}(\pi+\theta)^{\frac{\pi+\theta}{2\pi}}}\right]. \tag{31b}$$

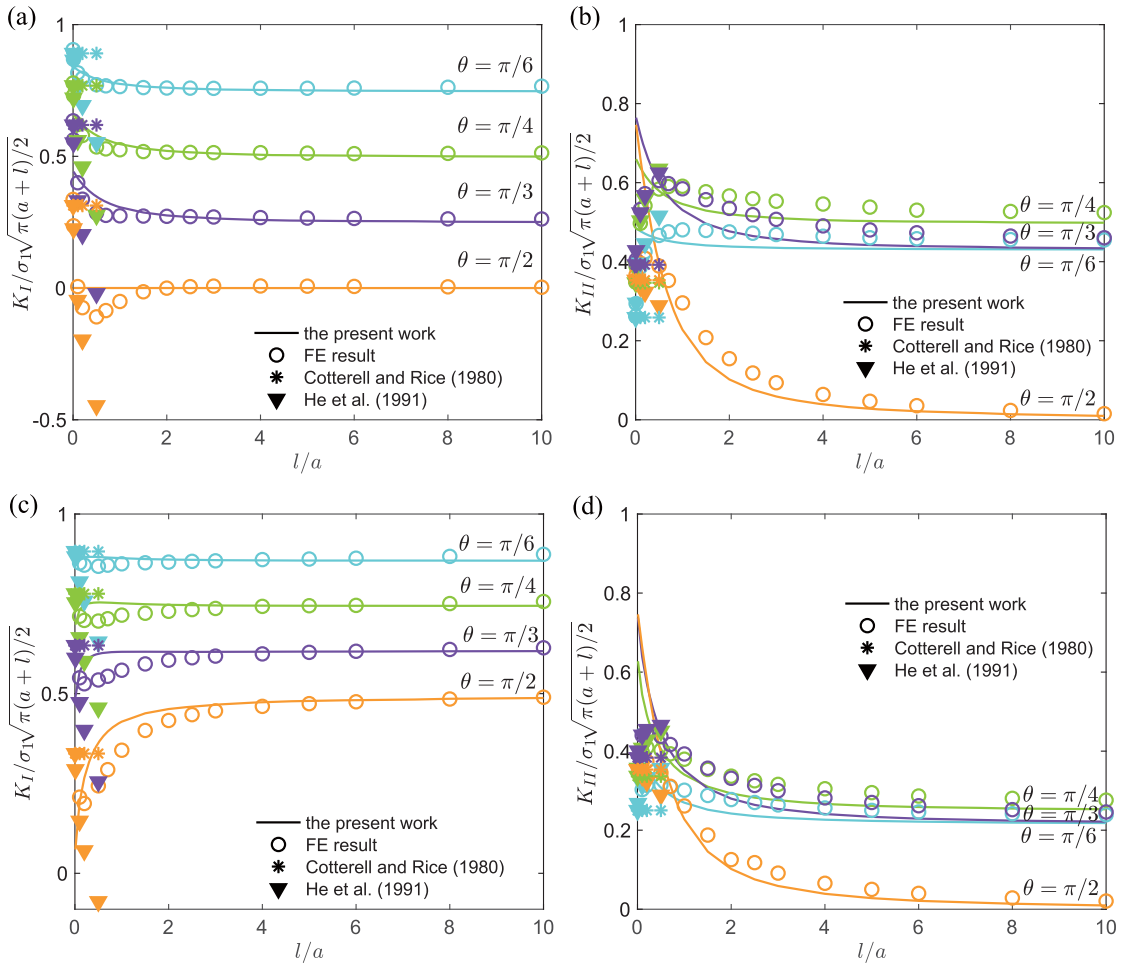

Fig. 7. A comparison of the stress intensity factors of kinked cracks among different methods: This work (solid lines), Cotterell and Rice (1980) (stars), He et al. (1991) (filled triangles) and the FE results (open cycles). (a) and (b), K_{I} and K_{II} as a function of l/a, respectively, uniaxial loading. (c) and (d), K_{I} and K_{II} vs. l/a, respectively, biaxial loading.

When $\theta = 0$, we can get $K_{\mathrm{I}} = \sigma\sqrt{\pi a}$ and $K_{\mathrm{II}} = 0$, which are exact the same as the SIFs of a straight crack with length $2a$. Fig. 8c shows again K_{I} and K_{II} as a function of θ. Now both Eq. (28) in this study performs better in contrast with predictions from Eq. (30) by He et al. (1991). In particular for K_{I}, our theoretical predictions match well with FE simulation results.

(1) When $l/a \to \infty$, we have

$$K_{\mathrm{I}} - iK_{\mathrm{II}} = \frac{1}{2}\sigma\sqrt{\frac{\pi l}{2}}\left(1 + e^{-2i\theta}\right) = \sigma\sqrt{\frac{\pi l}{2}}\left(\frac{1+\cos 2\theta}{2} - i\frac{\sin 2\theta}{2}\right). \tag{31c}$$

The formulae for K_{I} and K_{II} are in exact form of an inclined straight crack with length l and inclined angle θ with respect to the x-axis. The SIFs given by Eq. (28) capture what we obtain from FE results by setting $l/a = 10$ to approximate the theoretical formula when $l/a \to \infty$, as clearly demonstrated in Fig. 8d.

From Fig. 8, we see that Eq. (28) captures our FE results well when $l/a > 0.2$. When l/a is rather small, the crack-tip stresses of the kink may be overwhelmingly influenced by the K-dominance of the first crack. That may justify the effectiveness of the perturbation method in this region. Furthermore, we take for granted in Eq. (26) that both K_{I} and K_{II} follow a $1/\sqrt{r}$ singularity for kinked cracks, which may merit further exploration. Our theoretical solution, without knowing the stress fields from the first part of the double-kinked crack but taking both parts of the crack as a whole, may reflect the mathematical truth of the physically kinked crack. That is, our solution is for 'a single crack' with an abrupt kink.

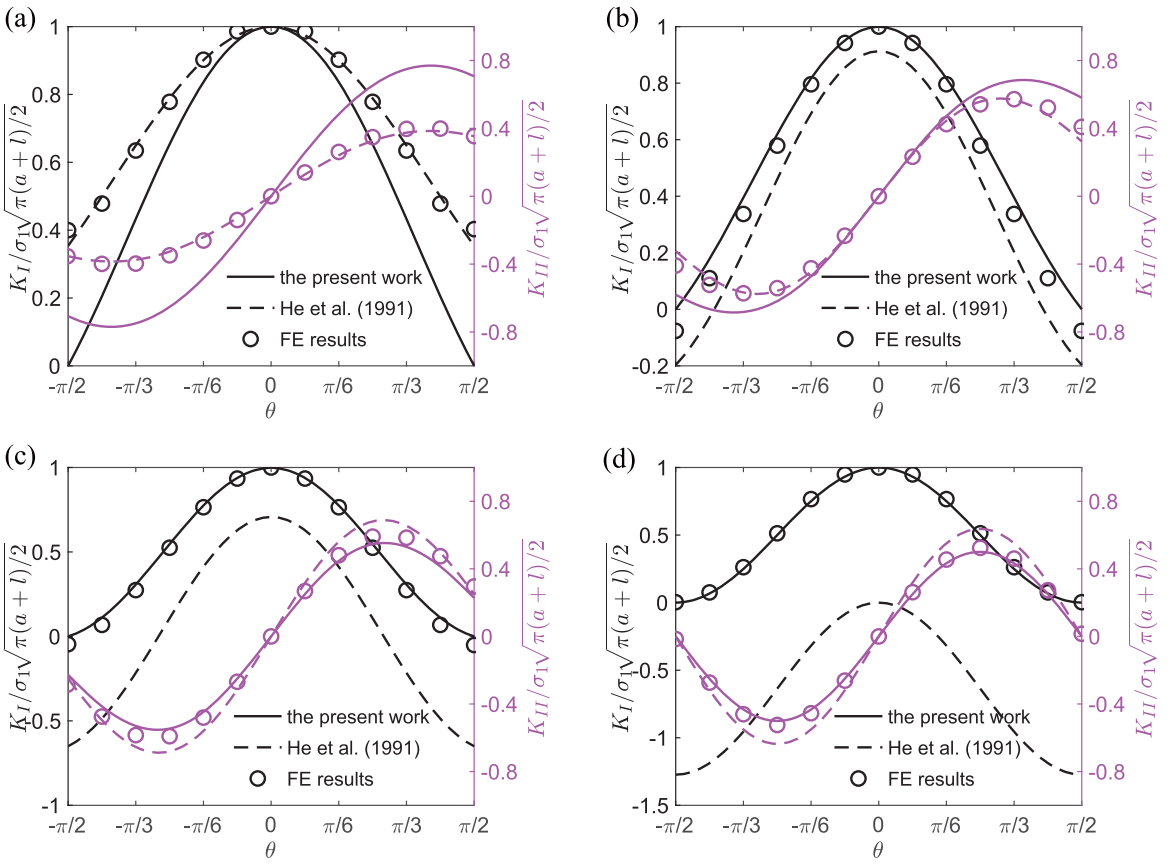

Fig. 8. A comparison of stress intensity factors vs. kink angle θ with a variety of l/a among different methods: This work (solid lines), He et al. (1991) (dotted lines) and the FE results (open cycles). (a) $l/a = 0$, (b) $l/a = 0.2$, (c) $l/a = 1$, and (d) $l/a \to \infty$.

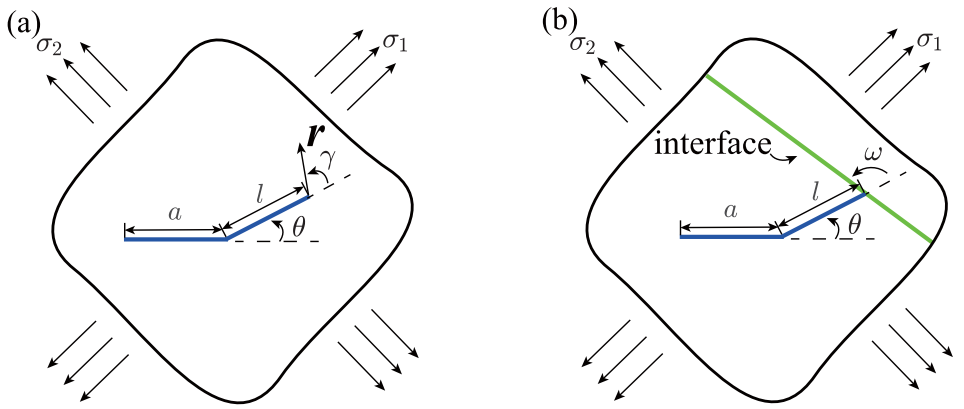

Fig. 9. Geometric information of a kinked crack. (a) The length of the original part a, the kink part l, the kink angle θ, and the potential deflecting angle γ. (b) The kinked crack running into an interface characterized by ω with repect to the kinked part.

4. The second crack deflection in brittle media

With the available SIFs given in Eq. (28) in the previous section, we now proceed to discuss more complicated case when a kinked crack running into a weak plane.

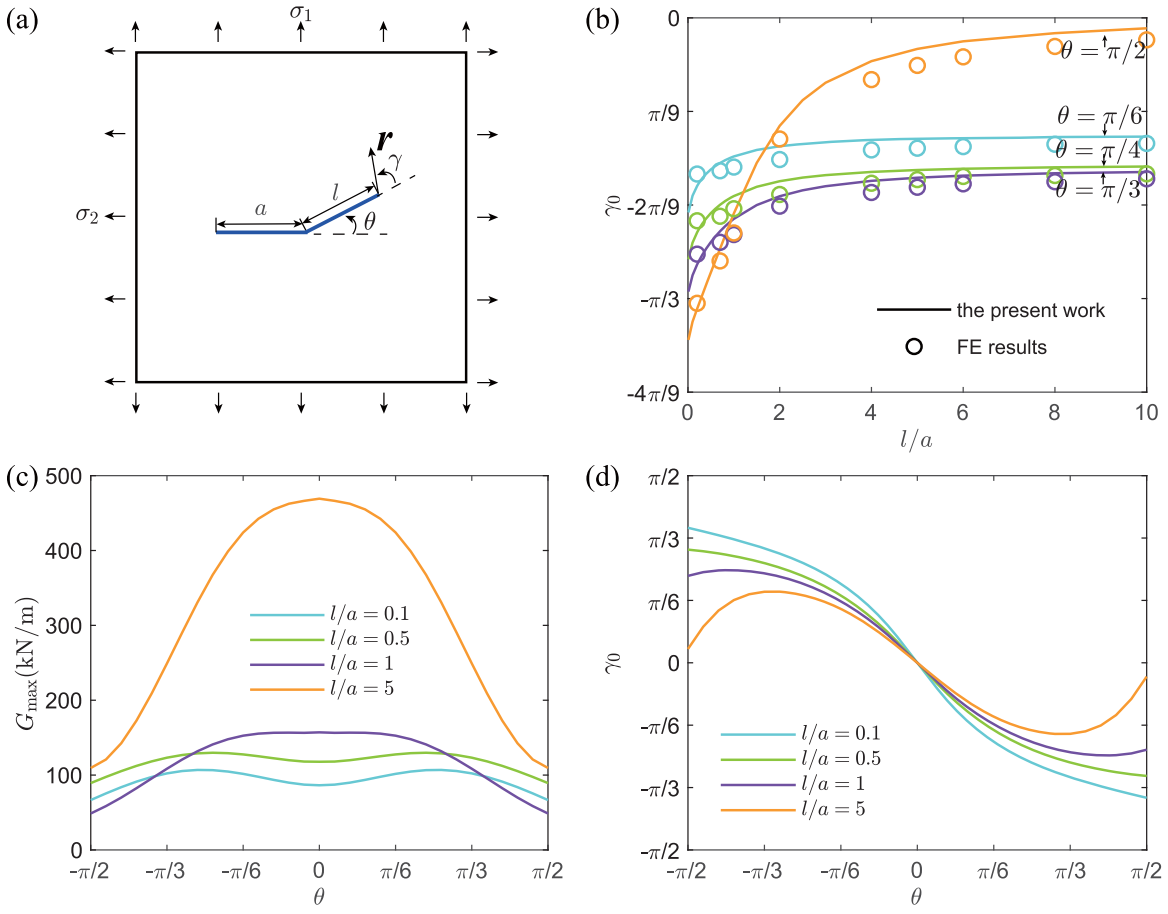

Fig. 10. Deflection of a kinked crack. (a) The geometrical information of a kinked crack in isotropic media under biaxial loading. (b) Comparison of the potential deflection angle γ_0, theoretical prediction (solid lines) vs. FE simulations (symbols). (c) The maximum strain energy release rate with respect to the kink angle θ for several l/a. (d) Potential deflection angle γ_0 vs. θ for a variety of l/a.

4.1. The second deflection in isotropic brittle materials

As demonstrated in the well-known work of Griffith (1921) on rupture, potential energy will release when a crack propagates, and it will go along the direction where the energy release the most (Cotterell, 1965). Based on these researches, maximum energy release rate criterion was developed to predict the crack propagation path in isotropic brittle materials (Hussain et al., 1973; Nuismer, 1975).

As we discussed in Section 3.2, the local stress fields at the tip of a kinked crack can use the expression of a straight crack given by Williams (1957). Therefore, the SIFs of a double-kinked crack shown in Fig. 9a with an infinitesimal second kink length at an angle γ are

$$K_{\mathrm{I}\gamma} = \frac{1}{2}\cos\frac{\gamma}{2}[K_{\mathrm{I}}(1+\cos\gamma) - 3K_{\mathrm{II}}\sin\gamma], \tag{32a}$$

$$K_{\mathrm{II}\gamma} = \frac{1}{2}\cos\frac{\gamma}{2}[K_{\mathrm{I}}\sin\gamma + K_{\mathrm{II}}(3\cos\gamma - 1)]. \tag{32b}$$

The strain energy release rate of this double-kinked crack at γ is (Zeng and Wei, 2017)

$$G_\gamma = \begin{cases} \dfrac{K_{\mathrm{II}\gamma}^2}{E^*}, & K_{\mathrm{I}\gamma} < 0 \\ \dfrac{K_{\mathrm{I}\gamma}^2 + K_{\mathrm{II}\gamma}^2}{E^*}, & K_{\mathrm{I}\gamma} \geq 0 \end{cases}, \tag{33}$$

where E^* is the modified elastic modulus, $E^* = E$ for the plane stress and $E^* = \frac{E}{(1-\nu^2)}$ for the plane strain. We substitute Eq. (32) into (33) and get

$$G_\gamma = \begin{cases} \dfrac{\cos^2\left(\frac{\gamma}{2}\right)\left[K_{\mathrm{I}}^2\sin^2\gamma + K_{\mathrm{II}}^2(3\cos\gamma-1)^2 + 2K_{\mathrm{I}}K_{\mathrm{II}}\sin\gamma(3\cos\gamma-1)\right]}{4E^*}, & K_{\mathrm{I}\gamma} < 0 \\ \dfrac{\cos^2\left(\frac{\gamma}{2}\right)\left[K_{\mathrm{I}}^2(1+\cos\gamma) + K_{\mathrm{II}}^2(5-3\cos\gamma) - 4K_{\mathrm{I}}K_{\mathrm{II}}\sin\beta\right]}{2E^*}, & K_{\mathrm{I}\gamma} \geq 0 \end{cases}. \tag{34}$$

The maximum strain energy release rate is determined by solving the equation $\frac{\partial G_\gamma}{\partial \gamma} = 0$. From which we have

$$G_{\gamma\max} = \frac{\cos^2\left(\frac{\gamma_0}{2}\right)\left[K_{\mathrm{I}}^2(1+\cos\gamma_0) + K_{\mathrm{II}}^2(5-3\cos\gamma_0) - 4K_{\mathrm{I}}K_{\mathrm{II}}\sin\gamma_0\right]}{2E^*}, \tag{35}$$

where γ_0 is

$$\gamma_0 = \begin{cases} -\arccos\left(\dfrac{3K_{\mathrm{II}}^2 + \sqrt{K_{\mathrm{I}}^4 + 8K_{\mathrm{I}}^2K_{\mathrm{II}}^2}}{K_{\mathrm{I}}^2 + 9K_{\mathrm{II}}^2}\right), & \text{for } K_{\mathrm{II}} \geq 0 \\ \arccos\left(\dfrac{3K_{\mathrm{II}}^2 + \sqrt{K_{\mathrm{I}}^4 + 8K_{\mathrm{I}}^2K_{\mathrm{II}}^2}}{K_{\mathrm{I}}^2 + 9K_{\mathrm{II}}^2}\right), & \text{for } K_{\mathrm{II}} < 0 \end{cases}. \tag{36}$$

Particularly, when $K_{\mathrm{I}} = 0$, $\gamma_0 = -\mathrm{sgn}(K_{\mathrm{II}})\arccos\left(\frac{1}{3}\right)$ with $\mathrm{sgn}(\cdot)$ being the sign function, and $\gamma_0 = 0$ when $K_{\mathrm{II}} = 0$. By denoting $K_a^2 = 3K_{\mathrm{II}}^2 + \sqrt{K_{\mathrm{I}}^4 + 8K_{\mathrm{I}}^2K_{\mathrm{II}}^2}$ and $K_b^2 = K_{\mathrm{I}}^2 + 9K_{\mathrm{II}}^2$, we have $\cos\gamma_0 = \frac{K_a^2}{K_b^2}$ and $\sin\gamma_0 = -\mathrm{sgn}(K_{\mathrm{II}})\sqrt{1-\frac{K_a^4}{K_b^4}}$. By substituting Eq. (36) into (35), we have

$$G_{\gamma\max} = \begin{cases} \dfrac{\left(K_a^2+K_b^2\right)\left[K_{\mathrm{I}}^2\left(K_a^2+K_b^2\right) + K_{\mathrm{II}}^2\left(5K_b^2-3K_a^2\right) + 4K_{\mathrm{I}}K_{\mathrm{II}}\sqrt{K_b^4-K_a^4}\right]}{4K_b^4E^*}, & \text{for } K_{\mathrm{II}} \geq 0 \\ \dfrac{\left(K_a^2+K_b^2\right)\left[K_{\mathrm{I}}^2\left(K_a^2+K_b^2\right) + K_{\mathrm{II}}^2\left(5K_b^2-3K_a^2\right) - 4K_{\mathrm{I}}K_{\mathrm{II}}\sqrt{K_b^4-K_a^4}\right]}{4K_b^4E^*}, & \text{for } K_{\mathrm{II}} < 0 \end{cases}. \tag{37}$$

Particularly, when $K_{\mathrm{I}} = 0$, $G_{\gamma\max} = \frac{4K_{\mathrm{II}}^2}{3E^*}$, and for $K_{\mathrm{II}} = 0$, $G_{\gamma\max} = \frac{K_{\mathrm{I}}^2}{E^*}$.

By substituting Eq. (28) into (37) and (36) we can obtain the maximum strain energy release rate $G_{\gamma\max}$ and the angle γ_0, which is the deflection angle based on the criterion of maximum strain energy release rate (Hussain et al., 1973). The verification of this solution in a biaxial stress status (see Fig. 10a) is shown in Fig. 10b. We consider a model case with $\sigma_1 = 50$ MPa, $\sigma_2 = 25$ MPa, $a = 1$ m and $E^* = 50$ GPa. The prediction given by Eq. (36) fits well with the FE results. As the kink length growing, the second deflection angle converges to the solution of an inclined straight crack with the inclined angle θ. In this loading condition, the second deflection angle is less than 0. According to the research of Erdogan and Sih (1963), a crack will propagate along the direction where $K_{\mathrm{II}} = 0$ eventually, which is parallel to the original crack in the stress status shown in Fig. 10a. The crack will propagate along a zigzag trajectory. The changes of maximum strain energy release rate and the second deflection angle with respect to kink angle θ at different l/a are shown in Fig. 10c and d. The results shown in Fig. 10d demonstrate that the second deflection angles are of different sign, which means the crack may prefer to extend in a zigzag path.

4.2. The second crack deflection angle when facing heterogeneous interfaces

As for heterogeneous materials, the problem become more complicated. Zak and Williams (1963) gave the theoretical solutions of a crack tip which is perpendicular to the bi-material interface under symmetric stress fields. Dundurs (1969) defined two parameters to quantify the elastic mismatch of two isotropic materials. Cook and Erdogan (1972) solved an elastic perpendicular crack-interface problem by an integral form using two Dundurs Numbers. They also research on the propagation path problem numerically by adopting the maximum stress criterion.

Based on the maximum strain energy release rate criterion adopted for homogeneous media (Hussain et al., 1973), He and Hutchinson (1989) developed a crack deflection criterion, which is particularly useful when crack facing bi-material interface. According to this criterion, a crack will deflect if the following two conditions are met:

(1) The strain energy release rate of the crack propagating along the interface should meet,

$$G_\omega = G_{dc}. \tag{38a}$$

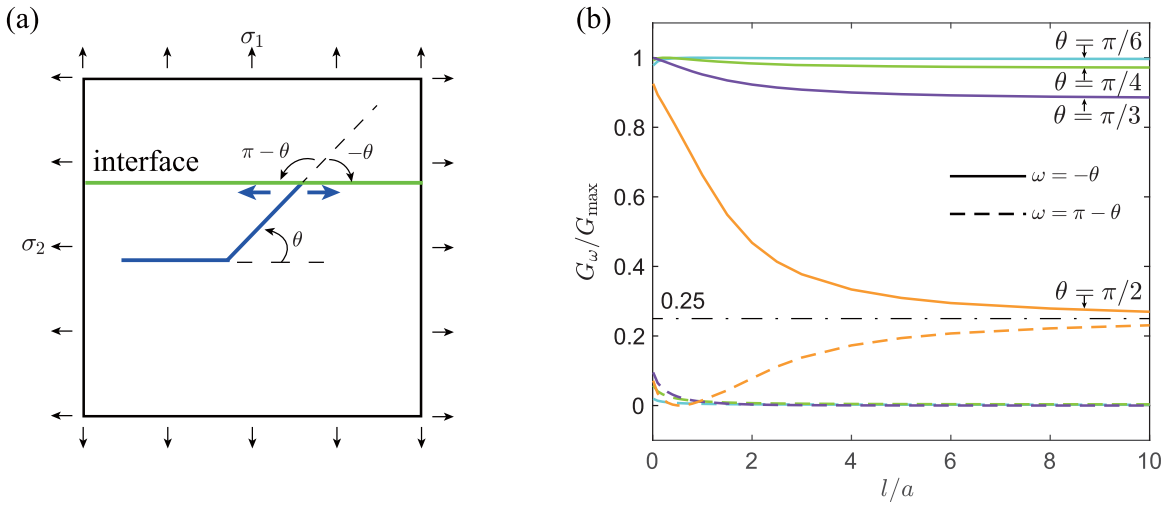

Fig. 11. A demonstration for the deflection of a kinked crack under biaxial loading. (a) The crack running into a heterogeneous interface parallel to its primary part, and (b) the normalized strain energy release rate $G_\omega/G_{\max}$ for the crack to deflect along both side of the interface.

(2) The ratio of strain energy release rate should meet,

$$\frac{G_\omega}{G_{\gamma\max}} > \frac{G_{dc}}{G_{mc}}, \tag{38b}$$

where G_{dc} and G_{mc} are the fracture toughness of the interface and the matrix, respectively. In the problem described in Fig. 9b, the strain energy release rate along the interface is

$$G_\omega = \begin{cases} \dfrac{\cos^2\left(\frac{\omega}{2}\right)\left[K_{\mathrm{I}}\sin\omega + K_{\mathrm{II}}(3\cos\omega - 1)\right]^2}{4E^*}, K_{\mathrm{I}\omega} < 0 \\ \dfrac{\cos^2\left(\frac{\omega}{2}\right)\left[K_{\mathrm{I}}^2(1+\cos\omega) + K_{\mathrm{II}}^2(5-3\cos\omega) - 4K_{\mathrm{I}}K_{\mathrm{II}}\sin\omega\right]}{2E^*}, K_{\mathrm{I}\omega} \geq 0 \end{cases}. \tag{39}$$

With Eq. (38) and (39), we have the normalized strain energy release rate as

$$\frac{G_\omega}{G_{\gamma\max}} = \begin{cases} \dfrac{2K_b^4\cos^2\left(\frac{\omega}{2}\right)\left[K_{\mathrm{I}}^2(1+\cos\omega) + K_{\mathrm{II}}^2(5-3\cos\omega) - 4K_{\mathrm{I}}K_{\mathrm{II}}\sin\omega\right]}{\left(K_a^2+K_b^2\right)\left[K_{\mathrm{I}}^2\left(K_a^2+K_b^2\right) + K_{\mathrm{II}}^2\left(5K_b^2-3K_a^2\right) + 4K_{\mathrm{I}}K_{\mathrm{II}}\sqrt{K_b^4-K_a^4}\right]}, \text{for } K_{\mathrm{II}} \geq 0 \text{ and } K_{\mathrm{I}\omega} \geq 0 \\ \dfrac{2K_b^4\cos^2\left(\frac{\omega}{2}\right)\left[K_{\mathrm{I}}^2(1+\cos\omega) + K_{\mathrm{II}}^2(5-3\cos\omega) - 4K_{\mathrm{I}}K_{\mathrm{II}}\sin\omega\right]}{\left(K_a^2+K_b^2\right)\left[K_{\mathrm{I}}^2\left(K_a^2+K_b^2\right) + K_{\mathrm{II}}^2\left(5K_b^2-3K_a^2\right) - 4K_{\mathrm{I}}K_{\mathrm{II}}\sqrt{K_b^4-K_a^4}\right]}, \text{for } K_{\mathrm{II}} < 0 \text{ and } K_{\mathrm{I}\omega} \geq 0 \\ \dfrac{K_b^4\cos^2\left(\frac{\omega}{2}\right)\left[K_{\mathrm{I}}\sin\omega + K_{\mathrm{II}}(3\cos\omega - 1)\right]^2}{\left(K_a^2+K_b^2\right)\left[K_{\mathrm{I}}^2\left(K_a^2+K_b^2\right) + K_{\mathrm{II}}^2\left(5K_b^2-3K_a^2\right) + 4K_{\mathrm{I}}K_{\mathrm{II}}\sqrt{K_b^4-K_a^4}\right]}, \text{for } K_{\mathrm{II}} \geq 0 \text{ and } K_{\mathrm{I}\omega} < 0 \\ \dfrac{K_b^4\cos^2\left(\frac{\omega}{2}\right)\left[K_{\mathrm{I}}\sin\omega + K_{\mathrm{II}}(3\cos\omega - 1)\right]^2}{\left(K_a^2+K_b^2\right)\left[K_{\mathrm{I}}^2\left(K_a^2+K_b^2\right) + K_{\mathrm{II}}^2\left(5K_b^2-3K_a^2\right) - 4K_{\mathrm{I}}K_{\mathrm{II}}\sqrt{K_b^4-K_a^4}\right]}, \text{for } K_{\mathrm{II}} < 0 \text{ and } K_{\mathrm{I}\omega} < 0 \end{cases}. \tag{40}$$

Here we give an application of Eq. (40). We consider a kinked crack under biaxial stress status, as shown in Fig. 11a. For demonstration, we consider the model case with $\sigma_1 = 50$ MPa, $\sigma_2 = 25$ MPa, $a = 1$ m, and the heterogeneous interface is parallel to the original part of the kinked crack. If the crack propagates along the interface, there are two possible choices, $\omega = -\theta$ and $\omega = \pi - \theta$. The normalized strain energy release rate obtained by Eq. (40) is given in Fig. 11b. When $\theta = \pi/2$, as $l/a \to \infty$, it becomes a symmetrically loading problem and the normalized strain energy release rates along both side of the interface given by Eq. (40) become the

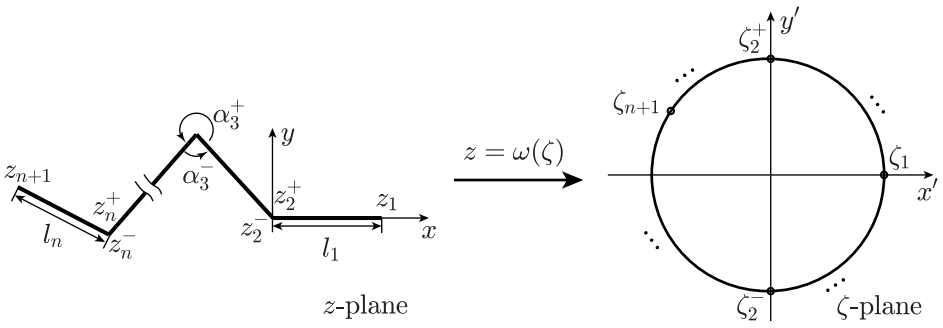

Fig. 12. The geometric information of a general multiple-kinked crack and its corresponding mapping (the unit circle).

same, which leads to $\frac{G_\omega}{G_{\max}} = \cos^4\left(\frac{\pi}{4}\right) = 0.25$, as being numerically given by He and Hutchinson (1989). Its rigorous proof was supplied by Zeng and Wei (2017). As we can conclude from Fig. 11b, a kinked crack in this loading condition has the potential to propagate to form a zigzag trajectory.

5. Discussions and conclusions

5.1. Stress intensity factors for a multiple-kinked crack

We have discussed in detail the method to obtain the SIFs of a double-kinked crack. Here we will discuss the SIFs of more general cases for cracks with multiple kinks, as shown in Fig. 12. We consider a multiple kinked crack with n segments, and each segment has two ends. The free ends of the first and the last segments are denoted by z_1 and z_{n+1}, respectively; the joining ends between the k-th and $(k+1)$-th segments are respectively denoted as z_{k+1}^+ and z_{k+1}^- on the top and bottom surfaces, and the angles between the k-th and $(k+1)$-th segments on the top and bottom sides are α_{k+1}^+ and α_{k+1}^-, respectively. The length of the k-th segment is l_k. As shown in the left of Fig. 12, by setting $z_1 = l_1$ and $z_2^+ = z_2^- = 0$, we define a coordinate system in z-plane. The region in the outside of the kinked line can be regarded as a polygon with one free end at infinity. Therefore, we may employ the Schwartz-Christoffel Integral in Eq. (5a) to describe the mapping between the kinked line in z-plane and the unit circle in ζ-plane.

Similar to the method we introduced for Eq. (6a), we have the mapping points ζ_1 and ζ_{n+1} for z_1 and z_{n+1}, respectively, ζ_k^+ and ζ_k^- for z_k^+ and z_k^-, respectively. The corresponding angles for these points are $\alpha_1 = \alpha_{n+1} = 2\pi$ for ζ_1 and ζ_{n+1}, respectively. For any given α_{k+1}^+, we have $\alpha_{k+1}^- = 2\pi - \alpha_{k+1}^+$. They are the characteristic angles associated with ζ_k^+ and ζ_k^-, respectively. Therefore, Eq. (5a) can be written as

$$\omega(\zeta) = K_1 \int \left\{ \frac{(\zeta-\zeta_1)(\zeta-\zeta_{n+1})}{\zeta^2} \prod_{k=2}^{n} \left[(\zeta-\zeta_k^+)^{\frac{\alpha_k^+ - \pi}{\pi}} (\zeta-\zeta_k^-)^{\frac{\pi-\alpha_k^+}{\pi}} \right] \right\} \mathrm{d}\zeta + K_2. \tag{41}$$

According to Driscoll and Trefethen (2002), we have $(2n-3)$ independent equations for $2n$ unknowns ($\zeta_1, \zeta_{n+1}, \zeta_k^+, \zeta_k^-$ for $k = 2\cdots n$). We may proceed by fixing three parameters and the rest will be fully determined. It is convenient to set $\zeta_1 = 1$, $\zeta_2^+ = i$ and $\zeta_2^- = -i$ as shown in the right part of Fig. 12. Once the $2n$ parameters are determined, the corresponding conformal mapping $z = \omega(\zeta)$ is available. By employing $\omega(\zeta)$, we can solve the BVP and obtain the two complex analytical functions $\varphi(\zeta)$ and $\psi(\zeta)$. The SIFs are determined by $\omega(\zeta)$, $\varphi(\zeta)$ and $\psi(\zeta)$.

5.2. Concluding remarks

Crack path is of great significance in engineering practice, either for safety control or in crack network formation. One of the core problems in widely used energy-based criteria is to find the SIFs of the crack. In this work we established a theoretical framework to calculate the stress fields and hence the SIFs of arbitrarily sized kinked cracks. By using Schwartz-Christoffel Integral to mapping the crack with multiple kinks in real space to a circle in complex plane, we are able to solve the boundary value problem and obtain the complex analytical functions, from which we can further deduce the SIFs of the crack tip. The accuracy of our method is verified by comparing its predictability for both stress fields and SIFs against FE results. In contrast to the theory of He et al. (1991), our theory exhibits excellent predictability for cracks with $l/a \geq 0.2$, and the formulae given by He et al. (1991) excels for kinked cracks with rather small l/a. Following the same approach used by Zeng and Wei (2017), we further analyze the deflection of a double-kinked crack in brittle isotropic media or media with heterogeneous interfaces. The theoretical analysis is also validated by comparing the theoretical predictions with results from FE analysis. In the end, we illustrate that the mathematical approach can be extended to solve the SIFs of general cracks of multiple kinks. We hence expect that the method shown here can serve as a convenient tool to analyze the propagation path of cracks in complicated shape. Furthermore, while we only solve the elastic problem for isotropic media, the framework associated with complex analytical functions $\varphi(\zeta)$ and $\psi(\zeta)$ can be extended to anisotropic materials with a rather

complicated form (Muskhelishvili, 1953).

Author contribution statement

Y. Wei conceived the project and designed the research; Z. Liu and Y. Wei developed the theory, analyzed data, and discussed the results; Y. Wei and Z. Liu wrote the paper.

CRediT authorship contribution statement

Zhuo-Er Liu: Formal analysis, Investigation, Validation, Visualization, Writing – original draft, Writing – review & editing. **Yujie Wei:** Formal analysis, Methodology, Supervision, Funding acquisition, Writing – original draft, Writing – review & editing.

Declaration of Competing Interest

The authors declare that they have no known competing financial interests or personal relationships that could have appeared to influence the work reported in this paper.

Acknowledgment

Y.W. acknowledges support from the NSFC Basic Science Center for \primeMultiscale Problems in Nonlinear Mechanics\prime (No. 11988102) and (No. 11790291), the Strategic Priority Research Program of the Chinese Academy of Sciences (XDB22020200), and CAS Center for Excellence in Complex System Mechanics.

Appendix. An alternative way to obtain SIFs

Here we give an alternative method to calculate the SIFs by using one complex analytical function $\varphi(\zeta)$. With the linear fracture mechanics assumption and for plane deformation, Williams (1957) gave the stress components at the crack tip as

$$\sigma_x = \frac{K_{\mathrm{I}}}{\sqrt{2\pi r}}\cos\frac{\theta}{2}\left(1-\sin\frac{\theta}{2}\sin\frac{3\theta}{2}\right) - \frac{K_{\mathrm{II}}}{\sqrt{2\pi r}}\sin\frac{\theta}{2}\left(2+\cos\frac{\theta}{2}\cos\frac{3\theta}{2}\right), \tag{A1.a}$$

$$\sigma_y = \frac{K_{\mathrm{I}}}{\sqrt{2\pi r}}\cos\frac{\theta}{2}\left(1+\sin\frac{\theta}{2}\sin\frac{3\theta}{2}\right) + \frac{K_{\mathrm{II}}}{\sqrt{2\pi r}}\sin\frac{\theta}{2}\cos\frac{\theta}{2}\cos\frac{3\theta}{2}. \tag{A1.b}$$

Let $K = K_{\mathrm{I}} - iK_{\mathrm{II}}$ and $z - z_1 = re^{i\theta}$, we have

$$\sigma_x + \sigma_y = \frac{2K_{\mathrm{I}}}{\sqrt{2\pi r}}\cos\frac{\theta}{2} - \frac{2K_{\mathrm{II}}}{\sqrt{2\pi r}}\sin\frac{\theta}{2} = \mathrm{Re}\left[K\sqrt{\frac{2}{\pi(z-z_1)}}\right] = 4\mathrm{Re}[\varphi'(z)]. \tag{A2}$$

According to the definition of SIFs, we have

$$K = 2\sqrt{2\pi}\lim_{z\to z_1}\sqrt{z-z_1}\varphi'(z). \tag{A3}$$

With the conformal mapping $z = \omega(\zeta)$, and note that $\omega(\zeta) - \omega(\zeta_1) \approx \frac{1}{2}\omega''(\zeta_1)(\zeta-\zeta_1)^2$, $\omega'(\zeta) \approx \omega''(\zeta)(\zeta-\zeta_1)$, $\omega'(1) = 0$ and $\zeta_1 = 1$, we may rewrite Eq. (A3) as

$$K = 2\sqrt{2\pi}\lim_{\zeta\to\zeta_1}\sqrt{\omega(\zeta)-\omega(\zeta_1)}\,\frac{\varphi'(\zeta)}{\omega'(\zeta)} = 2\sqrt{\pi}\,\frac{\varphi'(1)}{\sqrt{\omega''(1)}}. \tag{A4}$$

By substituting Eqs. (6b) and (18) into (A4), we can calculate the SIFs at the tip of any kinked crack. The solution given by Eq. (A4) is the same that given by Eq. (28)

References

Azhdari, A., Nemat-Nasser, S., 1992. Energy-release rate and crack kinking in anisotropic brittle solids. J. Mech. Phys. Solids 44, 929–951.
Bunger, A., Detournay, E., 2008. Experimental validation of the tip asymptotics for a fluid-driven crack. J. Mech. Phys. Solids 56, 3101–3115.
Chuprakov, D., Melchaeva, O., Prioul, R., 2014. Injection-sensitive mechanics of hydraulic fracture interaction with discontinuities. Rock Mech. Rock Eng. 47, 1625–1640.
Cook, T.S., Erdogan, F., 1972. Stress in bonded materials with a crack perpendicular to the interface. Int. J. Eng. Sci. 10, 677–697.
Cotterell, B., 1965. On brittle fracture paths. Int. J. Fract. Mech. 1, 96–103.
Cotterell, B., Rice, J.R., 1980. Slightly curved or kinked cracks. Int. J. Fract. 16, 155–169.
Detournay, E., 2016. Mechancis of hyraulic fractures. Annu. Rev. Fluid Mech. 115, 311–339.

Driscoll, T.A., Trefethen, L.N., 2002. Schwartz-Chritoffel Mapping. Cambridge University Press.
Dundurs, J., 1969. Edge-bonded dissimilar orthogonal elastic wedges under normal and shear loading. J. Appl. Mech. 36, 650–652.
Erdogan, F., Sih, G.C., 1963. On the crack extension in plates under plane loading and Transverse shear. J. Basic Eng. 85.
Fett, T., Pham, V.B., Bahr, H.A., 2004. Weight functions for kinked semi-infinite cracks. Eng. Fract. Mech. 71, 1987–1995.
Gao, H.J., Rice, J.R., 1986. Shear stress intensity factors for a planar crack with slightly curved front. J. Appl. Mech. 53, 774–778.
Griffith, A.A., 1921. The phenomena of rupture and flow in solids. Philos. Trans. R. Soc. London Ser. A 221, 163–198.
Hayashi, K., Nemat-Nasser, S., 1981. Energy-release rate and crack kinking under combined loading. J. Appl. Mech. 48, 520–524.
He, M.Y., Bartlett, A., Evans, A.G., Hutchinson, J.W., 1991. Kinking of a crack out of an interface: role of in-plane stress. J. Am. Ceram. Soc. 74, 767–771.
He, M.Y., Hutchinson, J.W., 1989. Crack deflection at an interface between dissimilar elastic-materials. Int. J. Solids Struct. 25, 1053–1067.
Hussain, M., Pu, S., Underwood, J., 1973. Strain energy release rate for a crack under combined mode I and mode II. In: Proceedings of the 1973 national symposium on fracture mechanics. ASTM International, pp. 2–28.
Hutchinson, J.W., 1990. Mixed-mode fracture mechanics of interfaces, Metal-Ceramic Interfaces. Acta-Scripta Metall. Proc. Ser. 295–306.
Hutchinson, J.W., Suo, Z., 1992. Mixed mode cracking in layered materials. Adv. Appl. Mech. 29, 63–191.
Irwin, G.R., 1957. Analysis of stresses and strains near the end of a crack traversing a plates. J. Appl. Mech. 29, 63–191.
Leblond, J., Karma, A., Ponson, L., Vasudevan, A., 2019. Configurational stability of a crack propagating in a material with mode-dependent fracture energy - part I: mixed-mode I+III. J. Mech. Phys. Solids 126, 187–203.
Lecampion, B., Desroches, J., 2015. Simultaneous initiation and growth of mutiple radial hydraulic fractures from a horizontal wellbore. J. Mech. Phys. Solids 82, 235–258.
Lee, H.P., Olson, J.E., Holder, J., Gale, J.F., Mayers, R.D., 2015. The interaction of propagating opening mode fractures with preexisting discontinuities in shale. J. Geophys. Res. 120, 169–181.
Li, Y., Sun, T., Gao, Q., Tan, C., 2018. A stress intensity factor estimation method for kinked crack. Eng. Fract. Mech. 188, 202–216.
Lo, K.K., 1978. Analysis of branched cracks. J. Appl. Mech. 45, 797–802.
Moes, N., Dolbow, J., Belytschko, T., 1999. A finite element method for crack growth without remeching. Int. J. Numer. Meth. Eng. 46, 131–150.
Muskhelishvili, N.I., 1953. Some basic problems of the mathematical theory of elasticity. Noordhoff.
Nuismer, R.J., 1975. Energy-release rate criterion for mixed mode fracture. Int. J. Fract. 11, 245–250.
Quaranta, L., Maddegedrara, L., M., H., 2019. Interaction of horizontally aligned coplanar 3D penny cracks under compression. J. Mech. Phys. Solids 131, 180–203.
Rice, J.R., 1968. A path independent integral and the approximate analysis of strain concentration by notches and cracks. J. Appl. Mech. 35, 379–386.
Rybicki, E.F., Kanninen, M.F., 1977. A finite element calculation of stress intensity factors by a modified crack closure integral. Eng. Fract. Mech. 9, 931–938.
Salvadori, A., Fantoni, F., 2016. Fracture propagation in brittle materials as a standard dissipative process: general theorems and crack tracking algorithms. J. Mech. Phys. Solids 95, 681–696.
Wei, Y.J., Gao, H.J., Bower, A.F., 2009. Numerical simulations of cracks deflection at a twist-misoriented grain boundary between two ideally brittle crystals. J. Mech. Phys. Solids 57, 1865–1879.
Weng, X., Kresse, O., Cohen, C., Wu, R., Gu, H., 2011. Modeling of hydraulic-fracture-network propagation in a naturally fractured formation. Soc. Pet. Eng. Prod. Oper. 26, 368–380.
Williams, M.L., 1957. On the stress distribution at the base of a stationary crack. J. Appl. Mech. 24, 109–114.
Yu, Y.L., Landis, C.M., Huang, R., 2018. Steady-state crack growth in polymer gels: a linear poroelastic analysis. J. Mech. Phys. Solids 118, 15–39.
Zak, A.R., Williams, M.L., 1963. Crack point stress singularities at a bi-material interface. J. Appl. Mech. 30, 109–114.
Zeng, X.G., Wei, Y.J., 2016. The influence of crack-orientation distribution on mechanical properties of pre-cracked brittle media. Int. J. Solids Struct. 96, 64–73.
Zeng, X.G., Wei, Y.J., 2017. Crack deflection in brittle media with heterogeneous interfaces and its application in shale fracking. J. Mech. Phys. Solids 101, 235–249.
Zhang, P., Ma, L., Fan, F., Zeng, Z., Peng, C., Loya, P.E., Liu, Z., Gong, Y., Zhang, J., Zhang, X., Ajayan, P.M., Zhu, T., Luo, J., 2014. Fracture toughness of graphene. Nat. Commun. 5, 3782.
Zhang, X., Jeffrey, R.G., 2006. The role of friction on secondary flaws on deflection and re-initiation of hydraulic fractures at orthogonal pre-exsiting fractures. Geophys. J. Int. 166, 1454–1465.
Zhang, X., Jeffrey, R.G., Thiercelin, M., 2007. Deflection and propagation of fluid-driven fractures at frictional bedding interfaces: a numerical investigation. J. Struct. Geol. 29, 396–410.
Zhao, J.H., Guo, W.L., 2012. Three-parameter K-T-Tz characterization of the crack-tip fields in compact-tension-shear specimens. Eng. Fract. Mech. 92, 72–88.
Zhu, T., Yang, W., 1999. Crack kinking in a piezoelectric solid. Int. J. Solids Struct. 36, 5013–5027.
Zou, Y., Ma, X., Zhang, S., Zhou, T., Li, H., 2016. Numerical investigation into the influence of bedding plane on hydraulic fracture network propagation in shale formations. Rock Mech. Rock Eng. 49, 3597–3614.